◆ Human Brain Mapping 31:1570–1587 (2010) ◆

Distortion Correction for Diffusion-Weighted MRI Tractography and fMRI in the Temporal Lobes

Karl V. Embleton,[1,2,3]* Hamied A. Haroon,[1,2] David M. Morris,[1,2] Matthew A. Lambon Ralph,[2,3] and Geoff J.M. Parker[1,3]

[1]*Imaging Science and Biomedical Engineering, School of Cancer and Imaging Sciences, University of Manchester, Manchester, M13 9PT, United Kingdom*
[2]*Neuroscience and Aphasia Research Unit, School of Psychological Sciences, University of Manchester, Manchester, M13 9PT, United Kingdom*
[3]*University of Manchester Biomedical Imaging Institute, University of Manchester, Manchester, M13 9PT, United Kingdom*

Abstract: Single shot echo-planar imaging (EPI) sequences are currently the most commonly used sequences for diffusion-weighted imaging (DWI) and functional magnetic resonance imaging (fMRI) as they allow relatively high signal to noise with rapid acquisition time. A major drawback of EPI is the substantial geometric distortion and signal loss that can occur due to magnetic field inhomogeneities close to air-tissue boundaries. If DWI-based tractography and fMRI are to be applied to these regions, then the distortions must be accurately corrected to achieve meaningful results. We describe robust acquisition and processing methods for correcting such distortions in spin echo (SE) EPI using a variant of the reversed direction *k* space traversal method with a number of novel additions. We demonstrate that dual direction *k* space traversal with maintained diffusion-encoding gradient strength and direction results in correction of the great majority of eddy current-associated distortions in DWI, in addition to those created by variations in magnetic susceptibility. We also provide examples to demonstrate that the presence of severe distortions cannot be ignored if meaningful tractography results are desired. The distortion correction routine was applied to SE-EPI fMRI acquisitions and allowed detection of activation in the temporal lobe that had been previously found using PET but not conventional fMRI. *Hum Brain Mapp 31:1570–1587, 2010.*

Key words: diffusion-weighted imaging; distortion; echo planar imaging; tractography; magnetic susceptibility; fMRI

INTRODUCTION

Single shot echo-planar imaging (EPI) is one of the fastest practicable magnetic resonance imaging methods and benefits from a high signal to noise ratio per unit time when compared with multishot imaging methods. As both diffusion-weighted imaging (DWI) tractography and functional magnetic resonance imaging (fMRI) usually have a requirement for a large number of image acquisitions, EPI has become the most popular choice for both neuroimaging methods. Although it has many advantages, EPI suffers from a low-pixel bandwidth in the phase-encode direction. This limitation results in EPI being prone to substantial geometric distortion and in the case of gradient

Contract grant sponsor: UK Medical Research Council; Contract grant numbers: G0300952, G0501632; Contract grant sponsor: UK Engineering and Physical Sciences Research Council; Contract grant number: GR/TO2669/01; Contract grant sponsor: UK Biotechnology and Biological Sciences Research Council; Contract grant number: BB/E002226/1.

*Correspondence to: Karl V. Embleton, ISBE, Stopford Building, University of Manchester, Oxford Road, Manchester, M13 9PT, United Kingdom. E-mail: karl.embleton@manchester.ac.uk

Received for publication 26 May 2009; Revised 1 October 2009; Accepted 2 November 2009

DOI: 10.1002/hbm.20959

Published online 8 February 2010 in Wiley Online Library (wileyonlinelibrary.com).

echo (GE) EPI (the sequence typically used for obtaining BOLD contrast in fMRI studies due to high sensitivity to T_2*) signal loss due to intravoxel dephasing when regions subject to large magnetic susceptibility variations are imaged, a problem that is intensified at higher magnetic field strength. Such regions of high-magnetic susceptibility variation occur around interfaces between different tissue types such as brain, bone, and air spaces. When single-shot EPI sequences are used to study brain regions close to these boundaries, for example, certain parts of the temporal lobes, these spatial intensity distortions are severe and have the potential to lead to erroneous and failed fiber tracking in DWI tractography and missing and misplaced coverage in functional data. Overcoming these distortion-related issues is critically important if the function and connectivity of such regions is to be systematically investigated. For example, neuropsychological studies have implicated the anterior temporal lobe in semantic memory, whereas the neuroimaging literature is relatively silent on this topic, in an extent due to technical issues involving the effects of magnetic susceptibility variations [Visser et al., in press].

A number of approaches have been suggested to achieve reductions in this magnetic susceptibility-related distortion including multishot, or segmented EPI, which may be used in place of single-shot EPI, with an associated reduction in echo train length and readout duration, leading to proportionally increased bandwidth and distortion reduction. The use of segmented EPI for DWI does, however, present a number of disadvantages, including longer scan times and difficulties with phase matching between shots caused by the large motion-induced phase evolutions resulting from the large diffusion sensitization gradients. Although the latter effect can be reduced using navigation [Miller and Pauly, 2003; Ordidge et al., 1994], segmented *k* space traversal is a fundamentally slower process than single-shot traversal. Another option for reducing distortions in EPI is to reduce the required echo train length using parallel imaging methods. This has been shown to be effective for EPI leading to levels of distortion reduction that are proportional to the parallelization factor utilized [Bammer et al., 2001, 2002]. Practically useful parallelization on standard commercial scanners is, however, generally limited to parallelization factors of approximately three or less at the present time, limiting the degree of distortion correction that is available via this method.

One popular approach to correcting distortion in EPI images is to use field mapping methods to map alterations to the magnetic field and to use this information to warp images to remove the ensuing distortions [Jezzard and Balaban, 1995; Jezzard et al., 1998]. Although field mapping techniques are capable of reducing distortion and may be of use in fMRI where exact location of signal is generally not as important as in DWI (smoothing and warping of images to a standard brain is usually applied to fMRI datasets), they are not capable of correcting for the signal pile up that occurs with EPI at higher fields, where a single voxel may contain the compressed signal from several other voxels in the phase encode direction. The correct repositioning of this signal depends upon the relative intensity of each of the original voxels, and this information is not present in field mapping corrections. Other described approaches include registration to structural images [Kybic et al., 2000; Studholme et al., 2000], local shimming [Clare et al., 2006; Du et al., 2007; Gu et al., 2002], compensation of signal and sensitivity losses by adjusting refocusing gradient amplitude for different image regions [Cordes et al., 2000], preparation gradient pulses designed to compensate for the effect of either positive or negative susceptibility gradients [Deichmann et al., 2002], inserting magnetic materials into subjects mouths [Cusack et al., 2005], measuring field inhomogeneities and adding factors to attempt to account for them to Fourier transforms [Liu and Ogawa, 2006], and parallel imaging [Preibisch et al., 2003; Schmidt et al., 2005; Yang et al., 2004]. Despite all this work, no single method for obtaining DWI and fMRI images in brain regions subject to high-magnetic susceptibility is in general use outside of the research organizations involved.

DWI using pulsed gradient spin echo (PGSE) EPI is additionally prone to distortions due to eddy currents induced in the scanner hardware by rapid switching of the large diffusion sensitization gradients. These eddy current-related distortions vary with strength and direction of diffusion gradient. The resulting distortion is seen as a combination of translation, shearing, and scaling factors in the phase encode direction [Jezzard et al., 1998]. A number of methods have been proposed for correcting this distortion including registration [Haselgrove and Moore, 1996] and modeling approaches [Andersson and Skare, 2002; Jezzard et al., 1998].

For an alternative method of distortion correction, we can consider the method of Chang and Fitzpatrick [Chang and Fitzpatrick, 1992] who described an approach for correcting minor spatial distortions due to magnetic field inhomogeneities in standard spin echo (SE) images. This was later applied to the more substantial distortions that occur in the phase-encoding direction of SE-EPI [Bowtell et al., 1994]. The correction relied on the acquisition of two images, identical except for positive or negative blipped gradient polarity. The resulting image pair showed equal degrees of distortion along matching phase encode direction profiles, although distortion occurred in opposite directions. By integrating the signal from corresponding profiles in the phase encode direction, matching cumulative intensity values could be found and the correct position of this intensity determined as the mean of the positions from the two cumulative distorted profiles. Further refinements of the technique have since been given [Morgan et al., 2004], including applications to DWI [Yoder et al., 2004].

We have implemented a version of the reversed gradient correction that allows us to routinely obtain high quality PGSE EPI DWI sets corrected for susceptibility and

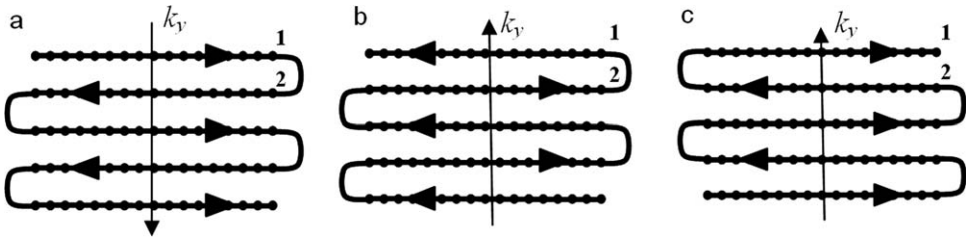

Figure 1.

k space traversal in (**a**) is the exact reversal of (**b**). Points 1 and 2 (and all other points) retain the same relative temporal positioning during acquisition and therefore the same magnitude accumulation of phase error. If only the phase-encoding gradient is reversed, as between (a) and (**c**), then the temporal spacing of points 1 and 2 in the k_y direction is also altered.

eddy current distortion and also allows distortion correction of SE EPI functional datasets corrected for geometric distortions and free of signal loss from intravoxel dephasing. We present here novel features of our acquisition and postprocessing protocol, which include an algorithm to detect signal voids in order to prevent integrating over background noise [Reinsberg et al., 2005] and a demonstration of how dual *k* space traversal without altering diffusion gradient direction can result in the correction of eddy current-related distortion.

Three different acquisition/postprocessing strategies for applying the correction to functional time series are examined using a functional task previously demonstrated to activate regions of the temporal lobe subject to high-magnetic susceptibility variations in a PET study [Devlin et al., 2000]. It is also demonstrated how the distortion in diffusion-weighted MRI can have a substantial effect on the output of tractography experiments in the temporal lobe and that our successful implementation of distortion correction produces substantial improvements.

METHODS

MRI Acquisition

All imaging was performed on a 3 T Philips Achieva scanner (Philips Medical Systems, Best, Netherlands) using an eight element SENSE head coil. A total of 12 subjects, age range 22–45, 6 male, 1 left handed, were scanned, with all sequences acquired in a single session lasting under an hour. All subjects gave informed consent, the study having been approved by the Local Research Ethics Committee. DWI was performed using a PGSE EPI sequence with TE = 54 ms, TR = 11884 ms, $G = 62$ mT m^{-1}, half scan factor = 0.679, 112 × 112 image matrix reconstructed to 128 × 128 using zero padding, reconstructed resolution 1.875 × 1.875 mm, slice thickness 2.1 mm, 60 contiguous slices, 61 noncollinear diffusion sensitization directions at $b = 1200$ s mm^{-2} (Δ, δ = 29.8, 13.1 ms), 1 at $b = 0$ s mm^{-2}, SENSE acceleration factor = 2.5. Each diffusion-weighted volume was acquired entirely before starting on the next diffusion weighting resulting in 62 temporally spaced volumes with different direction diffusion-encoding gradients. For each diffusion-encoding gradient direction, two separate volumes were obtained with opposite polarity *k* space traversal defined here as K_L and K_R (Fig. 1a,b, respectively). Note that although phase encoding was in the left–right direction, we maintain the conventional orientation in the *k* space diagrams with k_y vertical, for reader familiarity) and hence reversed phase and frequency encode direction. Total imaging time was 14 min for each polarity acquisition. Because of software limitations on the scanner, one complete set of diffusion images was acquired with one direction *k* space traversal and a second set of images then acquired with opposite direction traversal. This resulted in two image sets with a temporal separation of at least 14 min.

Parameters for functional imaging included sense factor of 2.5, 30 axial slices, interleaved slice order, TE = 75 ms, TR = 3200 ms, 112 × 112 matrix, reconstructed resolution 1.875 × 1.875 mm, and slice thickness 4.2 mm. Two fMRI acquisitions were made on each subject. Acquisition no. 1 consisted of 160 time points with interleaved alternate direction left–right/right–left (K_L and K_R) *k* space traversal with left–right phase-encoding. Acquisition no. 2 consisted of a prescan with interleaved dual direction phase encoding and the subject at rest (20 image volumes acquired, 10 for each direction *k* space traversal), followed by the main fMRI image sequence of 160 time points with a single phase-encoding direction over which the functional task was performed. Six of the subjects were imaged with acquisition no. 1 first and six with no. 2 first. Two of the time series from acquisition no. 1 were unusable due to scanner-related artefacts resulting in 10 usable datasets, 5 male, 5 female, all right handed, age range 22–45.

A colocalized T_2-weighted turbo SE scan with in-plane resolution of 0.94 × 0.94 mm and slice thickness 2.1 mm was also obtained as a structural reference scan to provide a qualitative indication of distortion correction accuracy.

Paradigm for Functional Study

The fMRI stimulus consisted of a word categorization task involving presentation of three sequential cue words

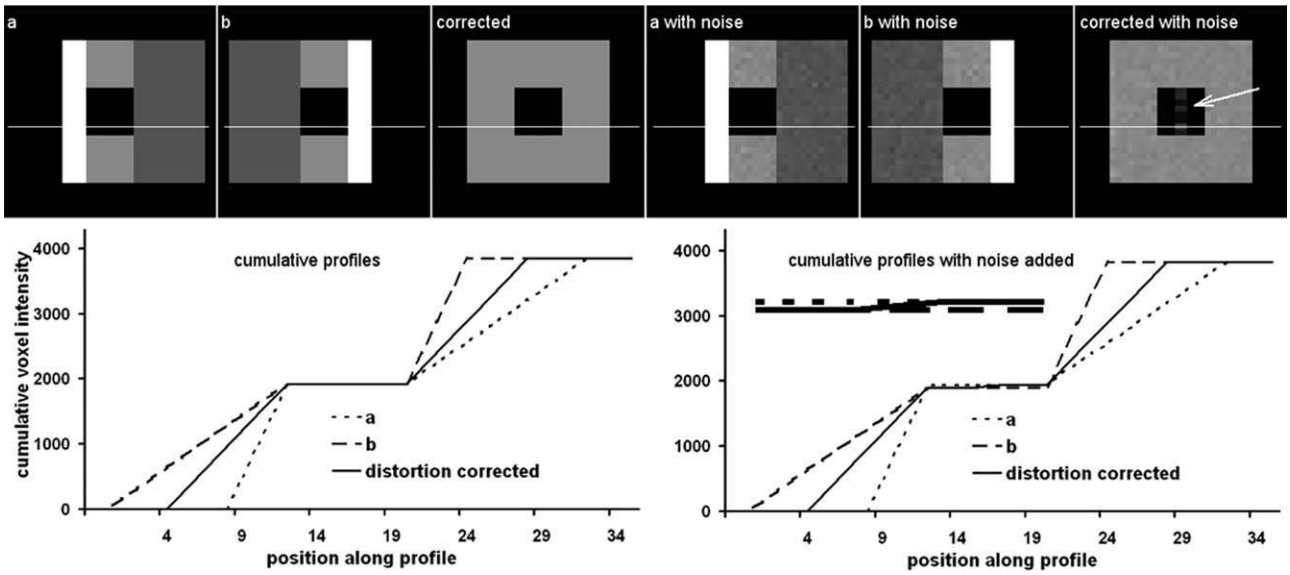

Figure 2.

Demonstration of the problem of signal voids using digital phantoms. Two digital phantoms, (**a**) and (**b**), with opposite direction distortion and signal compression/stretching (left–right direction) were created. With no noise added, the cumulative profiles (shown in the lower panel at the level of the horizontal white lines in the phantom images) match signal perfectly and the true correction is attained. After addition of noise (Gaussian noise with an SD of 4), the cumulative profiles show matching of signal on the left of the void in (b) with signal to the right of the void in a, as shown in the lower right panel. The heavy lines in this panel indicate a magnified area of the plot corresponding to the area of the signal void. This signal is erroneously placed into the center of the void in the corrected image (indicated by white arrow in corrected image with noise).

followed by a fourth underlined target word that required a rapid same/different decision as to whether it belonged to the same category as the cue words, for example, "knife," "spoon," "fork," and "spatula" (same) or "boat" (different). Subjects were instructed to press buttons with either index or middle finger of the right hand for same/different responses, respectively. All words were nouns describing nonliving objects and were from a previously used dataset [Devlin et al., 2000]. A letter categorization task with subjects presented with three strings of identical letters and a fourth underlined target string on which subjects were required to make a decision was used as a baseline condition.

Stimuli were presented in blocks of eight (eight trials per block, four same, four different categories, random order) with eight blocks each for word and letter categorization. Each block lasted for 32 s alternating between word and letter blocks. Each cue word (or letter string) was displayed for 200 ms with a 400-ms delay between them. The target word (or letter string) was also presented for 200 ms with a 2000-ms delay following the target word for subject responses to be made.

Distortion Correction for DWI

The fundamental steps in the distortion correction routine were based on those described in Bowtell et al. [1994] and our implementation included the following:

1. Images of the cumulative signal in the phase encode direction were derived allowing matching of cumulative signal between the K_L and K_R pair working on a profile at a time.
2. The subvoxel spatial positions for two matched cumulative signal values were estimated using cubic spline interpolation and a new profile constructed by placing the signal value at the mean position of the K_L and K_R profile positions. Matched values were found for each integer position in the cumulative signal (see Fig. 2).
3. The procedure was repeated for every profile in the phase encode direction to derive a corrected cumulative image which was then differentiated to noncumulative space.

Our full procedure included 3D six degrees of freedom registration to register each image volume to the first acquired diffusion-weighted volume and an algorithm to match corresponding segments separated by signal voids (e.g., CSF spaces in diffusion-weighted images) within profile pairs. This reduced propagation of errors along entire profiles and misplacing of corrected signal into signal voids. The problem of signal voids and misplaced signal is demonstrated using a digital phantom in Figure 2. The algorithm worked by splitting a profile into separate regions either side of signal voids, with the number of separate regions identical in both K_L and K_R images (Fig.

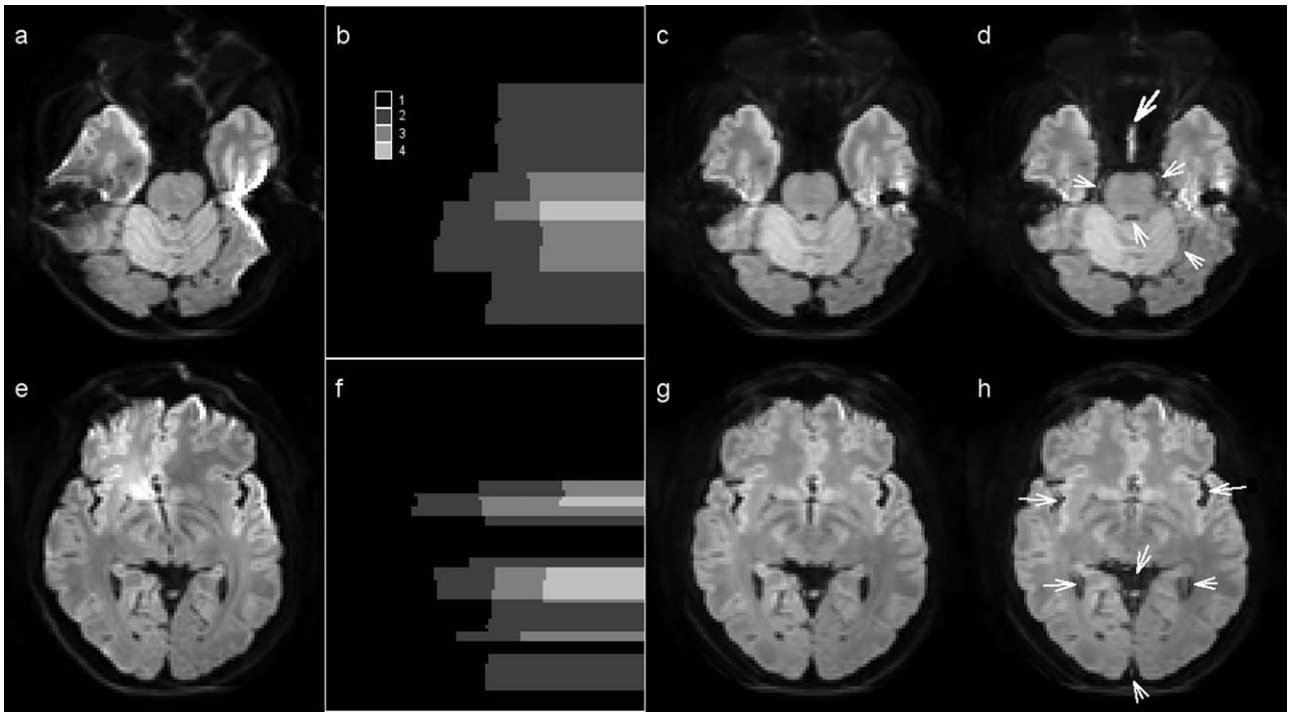

Figure 3.

Distortion correction with and without region matching algorithm. (**a, e**) are precorrection images, (**c, g**) are corrected using the region matching method, (**d, h**) without using region matching. All brain images are DWI mean intensity projections. The regions identified in the phase encode cumulative profiles are shown in (**b, f**). Arrows in (d, h) indicate incorrect repositioning of signal when region matching is not used. Large arrow indicates a particularly severe error.

3b,f). The matching of corresponding signal points in the cumulative profiles was then limited to each separate region by normalizing the intensity values in K_L regions with those in corresponding K_R regions. This region matching procedure required precise matching of profile segments from images displaying opposite distortion, a difficult problem in regions of severe distortion and signal pileup. To achieve this, an approximately-corrected $b = 0$ image was produced from the K_L and K_R images without any attempt to match regions of tissue. A template image (mean of 12 corrected $b = 0$ images from separate individuals) was registered to this image and the derived transform used to register two binary mask images, each approximately defining signal voids due to CSF in the ventricles in K_L and K_R images, into the diffusion space. These binary mask images were manually created from a mean image of 12 subjects and contained a matching number of regions along corresponding K_L and K_R profiles. A further routine then matched sections of each profile based on the subjects' own images. The $b = 0$ images were divided by the mean of the 61 diffusion-weighted images for both K_L and K_R imagesets to intensify the signal difference between CSF and other brain tissue (CSF has very high signal in the T_2 weighted $b = 0$ images yet very low signal in the DWI). This allowed CSF, the principle cause of signal voids in diffusion-weighted images (see examples in Fig. 3), to be accurately segmented using an empirically determined threshold (the same threshold value was robustly applicable to all subjects). The masks of CSF spaces were then used to break profiles into regions separated by CSF-related signal voids. The different regions along each profile pair were then compared to check that the number of regions in the K_L profile equaled that in K_R and that the total signal within each corresponding region was within 10%. If either of these checks was false, then the algorithm simply rejected the attempt to split the profile, and the profile was returned as a single region. A key point of note is that each region was progressively dilated along the profile until it bordered its neighbor, thereby ensuring that no signal was excluded overall. The separate profile sections identified in the second step were then added to the regions identified by the template registration. Matching of signal between the two line integrals was then limited to within these defined regions.

The correction procedure was applied to every pair of K_L and K_R of images for each slice and diffusion gradient orientation, a total of 3,720 image pairs for the diffusion-weighted protocol described earlier. All distortion

TABLE I. Functional acquisitions and corrected datasets

Functional data acquisitions				
1		Alternating k_L k_R direction k space traversal, 80 time points each direction, 160 time points in total		
2		k_L k_R prescan, subject at rest, 10 time points each direction, followed by functional scan with 160 k_L time points		
Distortion corrected datasets	Acquisition used	Correction method	Number corrected time points	Effective TR
A	1	k_L k_R pairs colocalization	80	6.4
B	1	Colocalization with next timepoint, corrected images temporally shifted	159	3.2
C	2	Colocalization correction on prescan, pixel shift applied to functional time series	160	3.2

correction code was written in Matlab (The MathWorks). The full procedure took around 2.5 h to run on a standard PC running Windows XP although no user input was required after initiation.

Distortion Correction for fMRI

Three methods for acquiring distortion-corrected functional data were compared and these required two separate functional acquisitions. Acquisition no.1 was corrected using two methods that we will refer to as A and B and acquisition no 2 was corrected as in C:

a. Each pair of images, K_{L1} and K_{R1}, K_{L2} and K_{R2}, were corrected following the reversed K space traversal colocalization of signal method as used for the diffusion imaging, except that identification of signal voids was limited to thresholds applied directly to the functional images, resulting in a series of 80 distortion-corrected images with an effective TR of 6,400 ms. Processing took around 15 min with no user input required after initiation.
b. Distortion-corrected images were achieved by correcting K_{L1} and K_{R1}, then K_{L2} and K_{R1}, K_{L2} and K_{R2}, K_{L3} and K_{R2}, etc. consecutively through the time series. This resulted in a dataset of 159 time points, maintaining an effective TR of 3,200 ms, although each corrected time point would be temporally smoothed between the two original images used in the correction. This temporal shift was entered into the FEAT (FSL, Oxford) functional analysis. Processing took around 30 min with no user input required after initiation.
c. A mean K_L and K_R image pair was produced from the 10 K_L and 10 K_R direction images in the prescan. This pair of images was then corrected as in A. During the correction process, a matrix of the shift applied to transform the mean K_L image (transforms worked on the cumulative images) into corrected space was obtained for intervals of 0.1 pixels in the phase-encoding direction resulting in a shift matrix of size 128 × 1280 × 30. The 160 time points in the functional acquisition, all direction K_L, were then corrected by first registering each 3D volume to the original distorted mean K_L volume using a 6 degrees of freedom translation and rotation algorithm (FLIRT, FSL) and then applying the matrix of pixel shift values to the registered images. This resulted in a distortion corrected dataset of 160 volumes maintaining the original temporal spacing and TR of 3,200 ms. The two acquisition strategies and three distortion correction methods are summarized in Table I. Processing took around 10 min with no user input required after initiation.

All three distortion-corrected datasets were subjected to statistical analysis using FEAT (FSL) with the following parameters selected: motion correction using MCFLIRT; spatial smoothing using a Gaussian kernel of FWHM 8 mm; mean-based intensity normalization of all volumes by the same factor; high-pass temporal filtering with a 64-s maximum temporal period; slice timing correction; time-series statistical analysis using FILM with local autocorrelation correction, registration to a standard image using FLIRT, and higher level fixed effects (FE) analysis. Clusters showing significant activation corrected for multiple comparisons at the whole brain level were identified using "Cluster" analysis with a range of Z statistic thresholds as indicated in Table II.

Comparison of Distortion Corrected and Uncorrected Functional Data

The FEAT analysis for functional results was repeated on acquisition 2 using the original uncorrected data to determine the effect of the distortion correction process on the statistical maps of activation. This comparison was limited to acquisition number 2 as the uncorrected data consisted of 160 time points, all with the same direction k space traversal and hence distortion, allowing easy functional analysis of the whole time series. Acquisition number 1 consisted of alternate direction distortion time points, and it was unfeasible to include the whole time

TABLE II. Results from functional analysis of corrected datasets

Z statistic threshold at voxel level	No. significant clusters $P < 0.05$			No. voxels in left inferior temporal lobe cluster			Max. Z statistic per cluster		
Correction method	A	B	C	A	B	C	A	B	C
2.327	1	1	3	1112	1227	8713	5.59	5.5	5.9
3.091	1	1	6	491	537	1423	5.59	5.5	5.9
3.719	1	1	7	246	275	737	5.59	5.5	5.9
4.265	1	1	8	123	137	126	5.59	5.5	5.9

series in a functional analysis without first performing the distortion correction process.

Comparisons between corrected and uncorrected data were made on the FEs higher-order analysis.

Tractography

To demonstrate the detrimental effect of distortion on tractography and the importance and effectiveness of the correction, we performed probabilistic tractography using the *PICo* method [Parker and Alexander, 2005; Parker et al., 2003] adapted to incorporate q ball [Haroon et al., 2009; Tuch, 2004] to discern multiple fiber orientations per voxel in both an original uncorrected and a corrected dataset. To ensure the same brain tissue was used as a seed region in both the distorted and distortion-corrected datasets the whole of the inferior right temporal lobe present within a single image slice was selected for unconstrained tracking (Fig. 4a).

We also performed simple streamline tractography using DTI-Studio (version 2.4.01, Johns Hopkins University, Baltimore) to demonstrate how distortion is detrimental to the propagation of individual streamlines (Fig. 4b). Two regions of interest were selected for both the left and right hemispheres separately. One region of interest enclosed the entirety of the temporal lobe on an inferior slice, and the second enclosed the temporal lobe on a lateral sagittal slice. All streamlines passing through both regions of interest were selected for each hemisphere. This streamline tractography was performed on a different dataset to that used for the probabilistic tractography in Figure 4a.

RESULTS

Correction of Susceptibility-Induced Distortions in EPI

Examples of SE-EPI images showing substantial distortion in the temporal and frontal lobes due to magnetic susceptibility effects are presented in Figure 5. The original EPI images show areas of substantial distortion with regions of very high intensity where signal has piled up from surrounding voxels. In the opposite k space traversal images, these areas show low intensity where corresponding signal has been stretched out. The gradient reversal-based process corrects virtually all of the substantial distortions that occur due to magnetic susceptibility differences in both the $b = 0$ and diffusion-weighted images, the only exception being a small region of intense signal pile-up that has not been completely resolved (indicated by arrows in Fig. 5g,h). Each distortion-corrected mean intensity projection in Figure 5h,p is created from 61 diffusion-weighted images with different direction diffusion gradients. The outlines of these mean intensity projections are well-defined, as eddy current distortion, which would otherwise be different for each individual gradient direction, has been corrected (see below). Figure 6b,d indicates very little difference in the quality of corrected images following application of methods A and C to the functional data. All three correction methods resulted in distortion corrected images showing close comparison with higher resolution TSE images.

Corrections performed both with and without the signal void region matching algorithm are illustrated in Figure 3. Arrows in 3d and 3h show regions where the distortion correction algorithm has misplaced signal when the region matching is not used. In Figure 3c,g, the definition between brain tissue and signal void due to CSF is much more clearly defined. The larger arrow in Figure 3d demonstrates an extreme case of signal misplacement where signal from opposite temporal lobes has been erroneously placed in the correction. This has been effectively corrected by the use of the region-matching algorithm.

Correction of Eddy Current-Induced Distortions

The single-shot PGSE EPI DWI sequence is prone to image distortions due to eddy currents that vary with diffusion-encoding gradient strength and orientation. This eddy current-induced distortion occurs in the form of translation, shearing, and a scaling away from the center of the image in the phase encode direction, resulting in different apparent brain perimeters for the 61 diffusion-weighted images, which can be visualized as a bright band around the perimeter of a generalized fractional anisotropy image [GFA; Tuch et al., 2003] (or any other anisotropy index). An example is shown in Figure 7a, in a brain slice with relatively little susceptibility-induced distortion. After application of the distortion correction

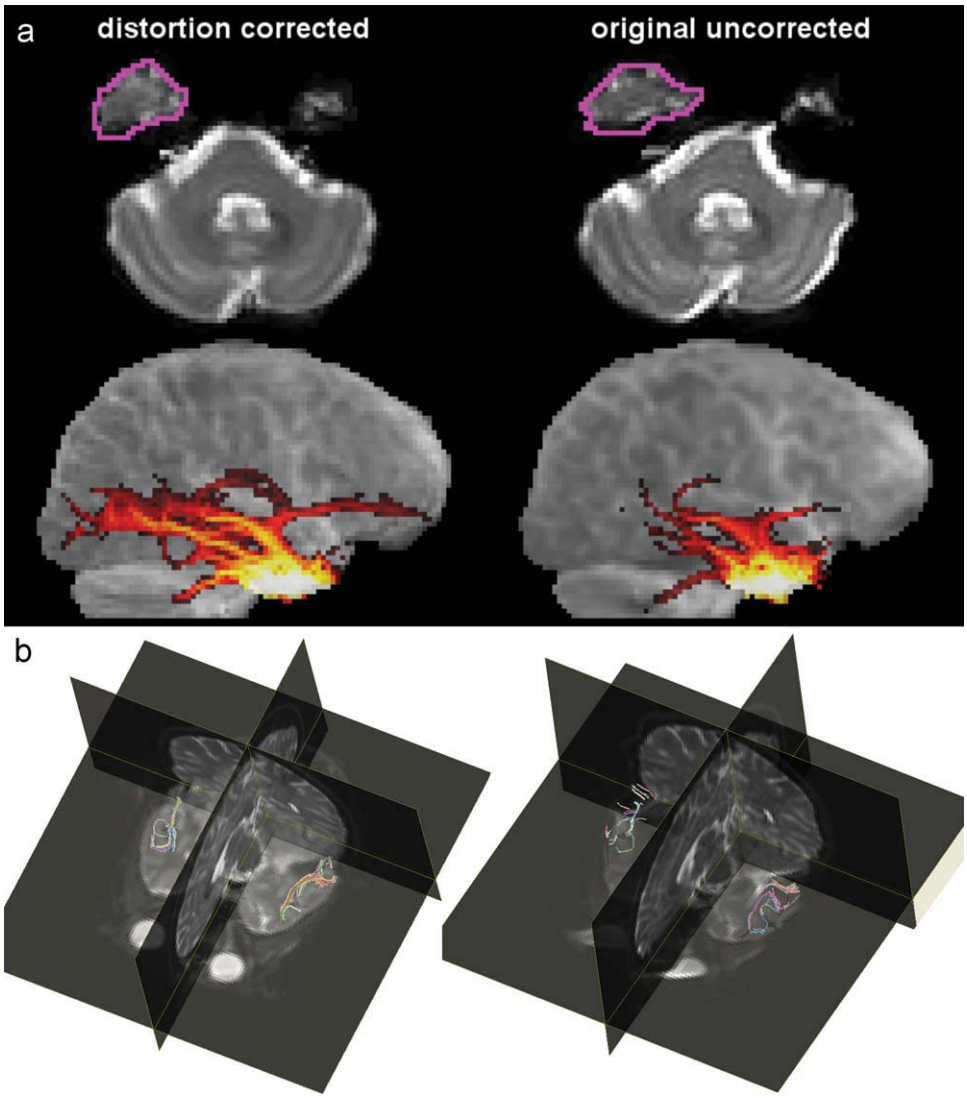

Figure 4.
Probabilistic tractography in distortion corrected and uncorrected datasets. Tractography was seeded from a region in the right inferior temporal lobe indicated by magenta borders. Tractography connection frequency was thresholded at identical levels and rendered as a maximum intensity projection.

algorithm, the brain perimeters of all 61 slices overlay correctly and the bright band surrounding brain matter in the GFA map has been effectively removed (Fig. 7b).

Influence of Distortion Correction on Tractography

The distortion correction algorithm greatly improves tracking through brain regions subject to susceptibility-related image distortions. This is illustrated in Figure 4a,b, where tractography results through the temporal lobe are shown for both original and distortion corrected data. Tract propagation is substantially improved in the distortion-corrected data as tract propagation breaks down in the region of misplaced orientation information demonstrated by an arrow in Figure 8 in the uncorrected data (the same dataset as Fig. 4a). Figure 8 also provides an illustration of the effects of distortion on fiber alignment in an idealized fiber tract.

Analysis of Functional Data from Subjects

The 8 min of functional data collection per individual in either of the functional acquisitions proved to have

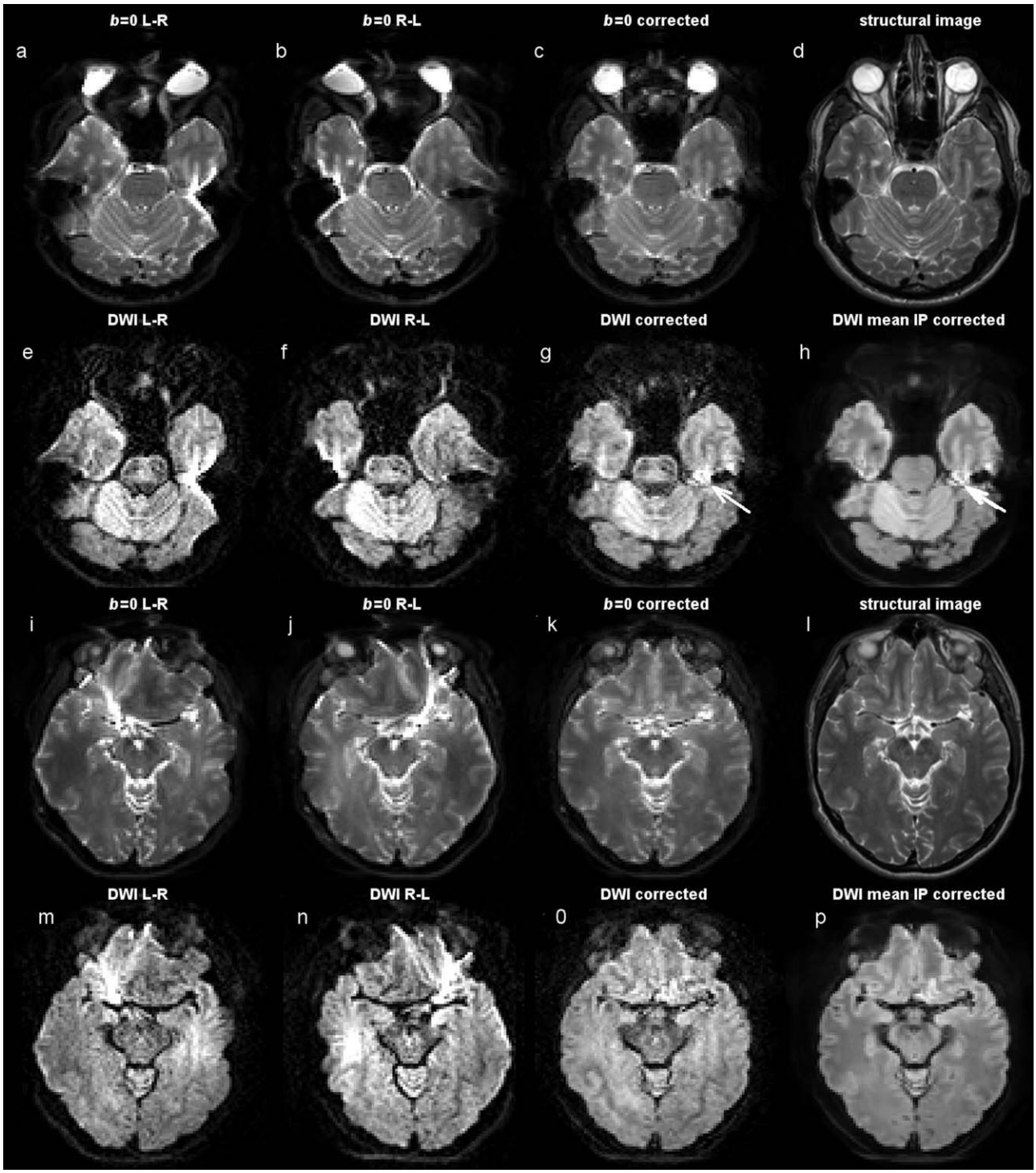

Figure 5.

Examples of diffusion weighted images before and after distortion correction. (**a, b, i, j**) $b = 0$ images with opposite polarity k space traversal, (**c, k**) corrected $b = 0$ images, (**d, l**) high-resolution TSE images for geometric comparison. (**e–g, m–o**) DW images pre and postcorrection. (**h, p**) DW mean intensity projections. Arrows indicate a small region where distortion has not been completely resolved in the corrected images.

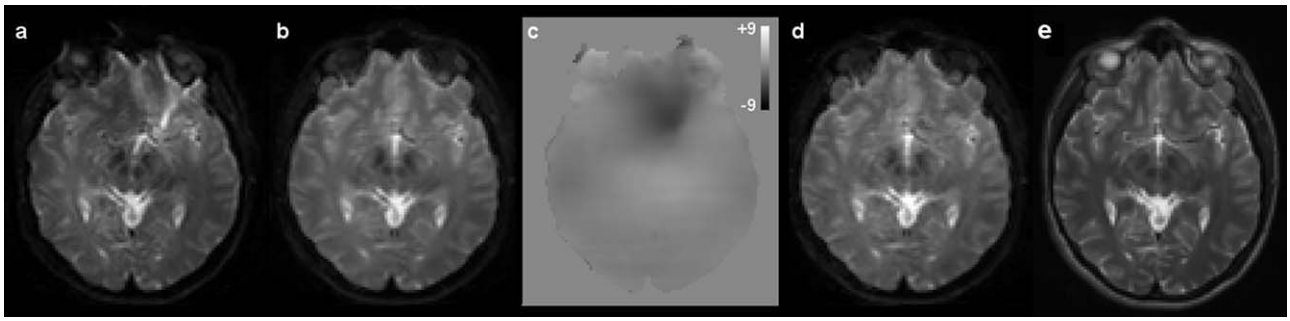

Figure 6.
Examples of distortion correction applied to functional images (**a**) example fMRI image, (**b**) fMRI prescan image corrected using reversed distortion pair, (**c**) map of pixel shift required to correct distorted fMRI image, (**d**) fMRI image from functional series after application of pixel shift map, and (**e**) high-resolution TSE image (resliced to same slice width as functional images).

insufficient statistical power for detecting activations (corrected for multiple comparisons) at the individual level. Comparisons of the three distortion correction methods applied to subject data were therefore limited to FEs analysis of data from all 10 subjects. The number of significant clusters (corrected for multiple comparisons) at $P < 0.05$ using a range of Z statistic thresholds are presented in Table II. Datasets A and B resulted in only one significant cluster at any of the Z statistic thresholds. In all cases, this cluster was in the left fusiform gyrus/inferior temporal lobe (see Fig. 9). Dataset C produced substantially more significant activation with three large clusters present at the lowest Z threshold and up to eight clusters using the highest.

The range of Z statistic values within the left fusiform cluster was examined by producing a Boolean AND mask for all three datasets and plotting the individual voxel Z scores. There is evidence that method C resulted in a shift toward higher Z scores (see Fig. 10).

Comparison of Distortion Corrected and Uncorrected Functional Data (Acquisition 2)

Both the distortion corrected and nondistortion-corrected datasets were subjected to a higher-order group analysis using cluster analysis to determine significant clusters with a Z-statistic threshold >3.719 and cluster

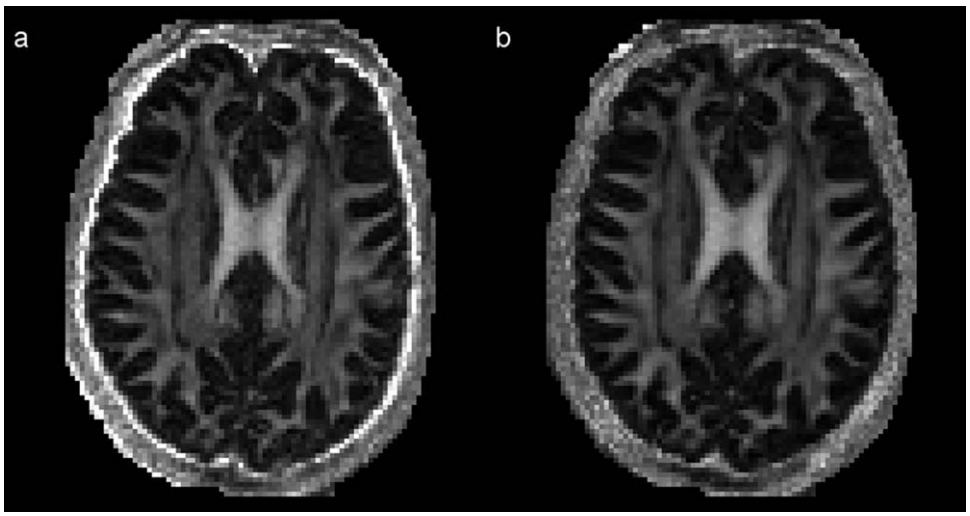

Figure 7.
(**a**) Generalised fractional anisotropy (GFA) image generated from a diffusion-weighted sequence with no susceptibility-induced or eddy current-induced distortion corrections applied, note bright band around periphery due to eddy current distortion. (**b**) GFA image from dual *k* space traversal distortion-corrected data. A slice with little susceptibility related distortion was chosen to better observe the effects of eddy currents.

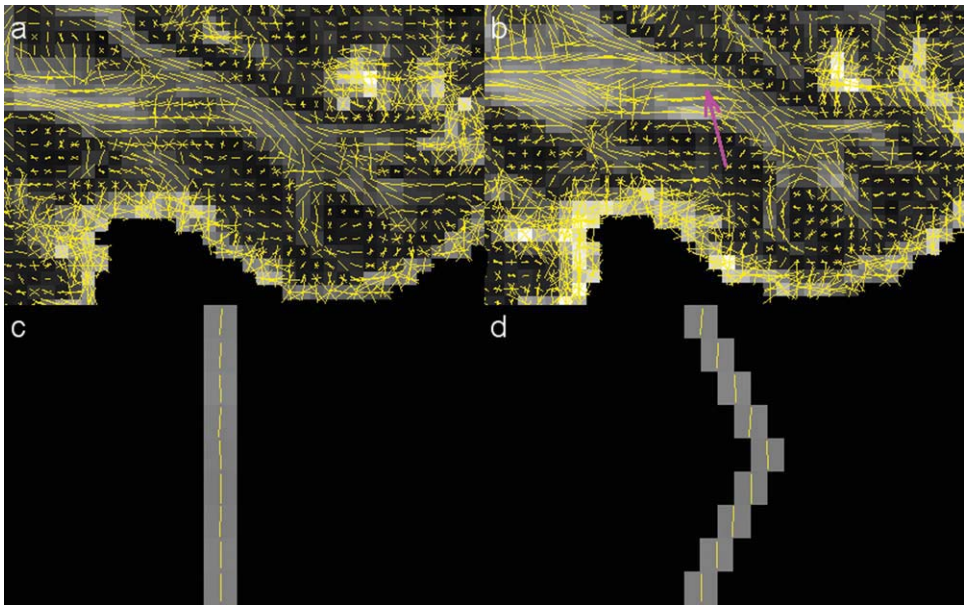

Figure 8.

(**a, b**) Examples of voxel-level fiber orientations in right temporal lobe using distortion corrected (a) and uncorrected data (b). Yellow lines represent major diffusion directions for each voxel, as extracted using the *q* ball algorithm, modulated by and overlaid on GFA maps. Long tracts descending through the temporal lobe with diffusion vectors in alignment (after correction) are present in (a), these tracts are disrupted by susceptibility distortion in (b) (magenta arrow). (**c**) Schematic of a tract in undistorted space with the calculated diffusion vectors running along an undistorted idealized tract. (**d**) The same tract as in (c) with the central portion misplaced due to susceptibility distortion. The gray levels and vector directions remain largely unchanged, although the vectors and the main axis of the tract are no longer in alignment.

$P > 0.05$. The distortion corrected data produced seven significant clusters and the nondistortion-corrected data produced nine clusters (Table III). Because of different sizes of activating areas and a minimum of voxels required for significant clusters, two ROIs in the corrected data were not present in the nondistortion-corrected data and four in the nondistortion-corrected data not present in the distortion corrected data. Corresponding regions thresholded at a Z statistic of >3.719 could be found for these ROIs, although not with a significant voxel number. Comparisons were therefore made between all clusters, although some of the clusters did not attain a volume sufficient to be significant when corrected for multiple comparisons over the whole brain. The cluster positions are given in Table III and Figure 11.

In general, statistics for the distortion corrected data were very close to those from the raw, nondistortion-corrected data. Notable exceptions were Clusters 5 and 6 where volume, max, and mean Z statistic were substantially higher in the distortion corrected data, especially in Cluster 6 located in the anterior part of the inferior temporal lobe, a region subject to very substantial distortion.

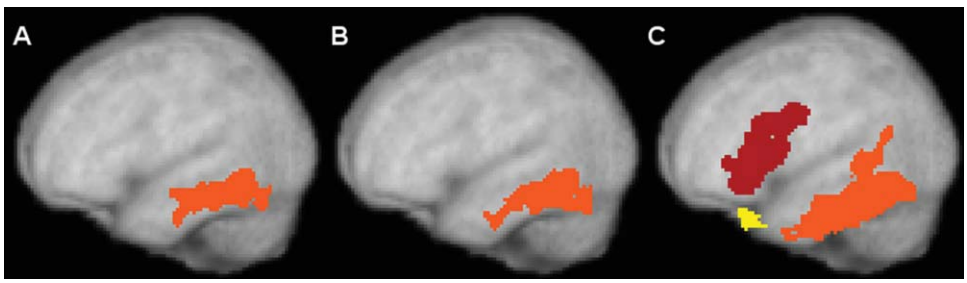

Figure 9.

Significant fMRI activations following three correction methods A, B, and C. Clusters significant at $P < 0.05$, $Z > 2.327$.

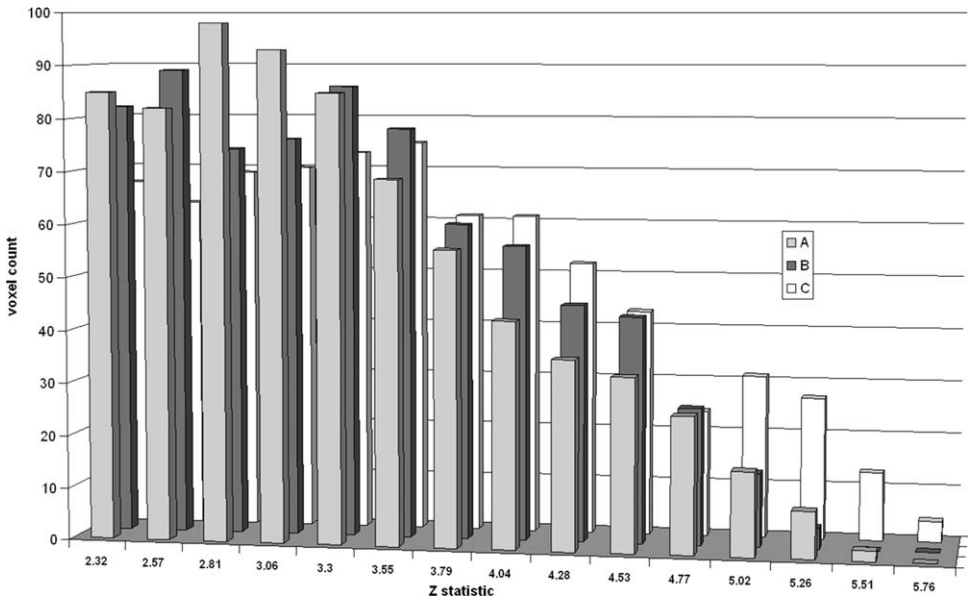

Figure 10.
Voxel level *Z* statistics from the fusiform gyrus cluster, comparison of the three datasets A, B, and C.

Clusters 8–10 were all smaller in the distortion corrected data and below the size required for statistical significance.

In comparison with an earlier study using the same functional task (see Fig. 12), substantially more activations were revealed in this work using SE EPI than were found with either PET or GE EPI fMRI in the original study [Devlin et al., 2000].

DISCUSSION

We have clearly demonstrated that the reversed *k* space traversal technique can be used to correct for in-plane geometric distortions caused by magnetic susceptibility effects in diffusion-weighted MRI and SE EPI fMRI and have presented a methodology that provides robust data acquisition and processing. We have also demonstrated that the methodology is suitable for removal of eddy current-induced distortion and has a positive effect on fiber tracking in areas subject to high levels of distortion.

There are, however, limits to the amount of distortion that can be corrected using this method [Morgan et al., 2004]. Most importantly, the presence of signal pile up in both the left and right profiles that overlap spatially in each distorted image represents a situation for which this method has no solution as the required signal-spatial information is simply not present. We therefore took steps

TABLE III. Comparison between activation clusters in data distortion corrected using method C (cor.) and nondistortion-corrected data (un)

		Cluster probability		Mean Z statistic		Maximum Z statistic		Cluster size (voxels)	
Cluster	Description	cor.	un.	cor.	un.	cor.	un.	cor.	un.
1	R frontal inf. oper.	0.042	0.0093	4.135	4.211	4.816	4.986	68	122
2	L frontal inf. orbit	0.026	0.0076	4.137	4.242	4.720	5.343	81	127
3	L precentral	0.0082	0.015	4.386	4.288	5.597	5.159	116	104
4	R insula	0.0031	0.0014	4.465	4.453	5.900	5.814	148	189
5	R putamen	0.0015	ns	4.264	3.978	5.254	4.392	175	65
6	R inf. temporal lobe	0.00031	ns	4.210	3.903	5.446	4.043	234	7
7	L inf. temp. lobe/fusiform	$<1 \times 10^{-7}$	$<1 \times 10^{-7}$	4.385	4.389	5.870	5.880	737	788
8	R cingulum mid.	ns	0.039	4.027	4.0358	4.483	4.657	48	75
9	R cerebellum Crus 1	ns	0.031	3.907	4.0635	4.145	4.768	17	82
10	R occipital mid./sup.	ns	0.013	4.033	4.25	4.430	5.220	47	110

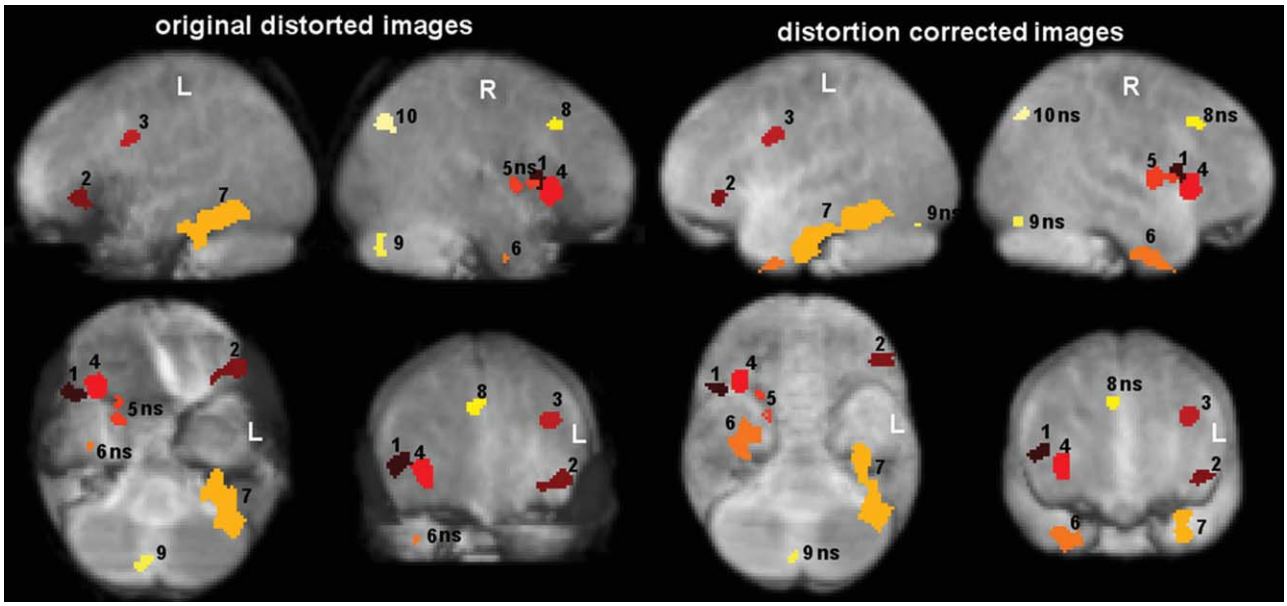

Figure 11.

Location of clusters in higher level analysis of original distorted and distortion corrected data. *Z* statistic threshold $P < 0.0001$, clusters significant for whole brain correction at $P < 0.05$ unless labeled with ns.

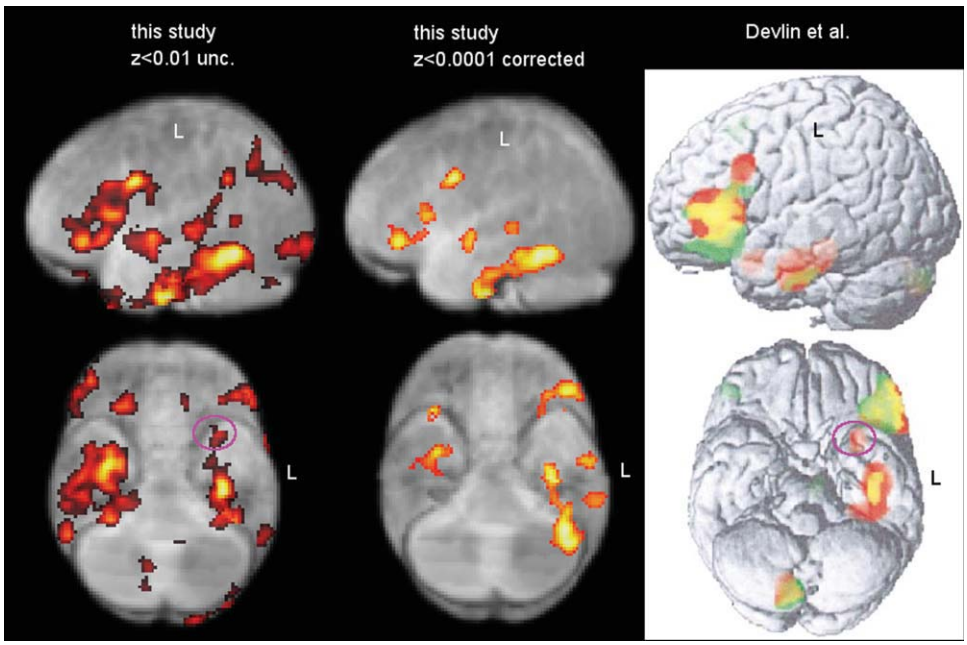

Figure 12.

Comparison of activation between the SE EPI used in this study and PET and GE EPI used by Devlin et al. (2000). In the Devlin data, PET activations are in red and fMRI in green with overlap in yellow. N.B. the renderings of SE EPI activations used an increased depth rendering in the corrected results compared with the uncorrected. SE EPI data is: left column $P < 0.01$, minimum extent 40 voxels, uncorrected for multiple comparisons, middle column $P < 0.0001$, clusters corrected for multiple comparison $P < 0.05$. Magenta circle indicates an activating region found using PET and present in our SE EPI fMRI, but not at a level surviving correction for multiple comparisons.

to reduce piling up of signal at the point of acquisition, which included the use of parallel imaging with a SENSE acceleration factor of 2.5 and phase encoding in the right–left direction rather than the more commonly utilized A-P (note that the main reason for the common usage of AP phase encode is to make the distortions symmetrical between cerebral hemispheres, a consideration that disappears when applying distortion correction). The benefits of right–left phase encoding for our correction method are first that it allows the use of a rectangular field of view with a reduced number of phase-encoding lines, thereby allowing a smaller echo train length, which proportionately reduces distortion. Second, the eyes are removed from the large majority of phase encode profiles used for the correction procedure. Eye movement will continuously occur during scanning, and alterations in eye position between image pairs will cause problems in profiles containing signal from the eyes should the phase encoding be in the AP direction.

Of critical importance to the accuracy of the distortion correction is the matching of signal from the same profile isochromat within the image pairs. Errors in matching cumulative signal accumulate along the profiles and will adversely affect the accuracy of the correction. Defining brain boundary positions over which the paired profiles are integrated should theoretically improve colocalization of signal in profile pairs and a mask defining only brain may be used for this purpose [Morgan et al., 2004]. In regions where susceptibility-induced distortion is substantial, we have found that accurately defining a mask fitting all 61 diffusion-weighted images while encompassing the exact same quantity of background in each K_L K_R pair is a difficult and time-consuming task, made all the more difficult by the influence of eddy current-related distortions, which alter the position of brain/nonbrain boundaries between different diffusion weightings.

When K_L K_R signal intensity profiles used for distortion correction contain two or more distinct regions of signal with a void between them (an example is found in diffusion-weighted images at the level of the ventricles where very low single of cerebral spinal fluid in diffusion-weighted images creates an apparent signal void), problems with misplaced signal in the corrected profile can arise. This misplacement of signal occurs as it is possible in noisy conditions for signal adjacent to the left of a signal void in a K_L cumulative profile to be matched with signal from the right of the void in the K_R cumulative profile and then to be erroneously repositioned into the center of the signal void in the corrected profile (see Fig. 3). To overcome this problem, we developed the region-matching algorithm to define corresponding blocks of tissue in profile pairs. To avoid mismatched sums in the total integrals, the two profiles require intensity normalization. By performing this normalization between corresponding sections of the profile as separated by the signal voids, the algorithm will automatically limit signal matching to corresponding sections and the incorrect positioning of signal into regions of very low signal will not occur. Finding an exact match of all the signal voids between the two image pairs is not an easy task in regions subject to high-spatial distortion as gaps in one image may be filled by distorted signal in the other. The greatest problems tend to occur in diffusion-weighted images in the region of the third and fourth ventricles where there are a number of regions of very low signal in the diffusion-weighted images due to CSF and where susceptibility-related distortion is very severe. Obtaining a satisfactory correction in this region required the use of the preprepared templates as the threshold-based correction was prone to failure due to uneven identification of signal voids between profiles. For the majority of the remaining brain, the automated identification of signal voids worked very well. As the borders between regions fell into the center of a signal void, the exact location of this border was not critical and small differences in boundary positions between diffusion weightings, due to the distortions from eddy currents, did not cause a major problem. When the correction procedure is applied to functional datasets the problem with signal voids is much reduced as CSF has high signal and therefore, there are few signal voids within the brain.

Although this algorithm to break profiles into separate sections interspersed with signal voids proved successful, it is perhaps an inelegant solution to the problem. Reinsberg et al. [2005] used the gradient reversal correction to correct for the minor spatial distortions occurring in nonecho planar imaging, in respect to surgical planning. They used maximization of mutual information to identify corresponding pixel positions between profiles and thereby overcoming the problem of signal voids and noise in the integrals. The images they were correcting were higher resolution than our echo planar images and suffered distortions that were only a tiny proportion of those experienced in EPI. Our attempts to apply their methods to our EPI data have so far failed as the profiles are too dissimilar, and the algorithms are unable to successfully match sufficient points.

In addition to correction of distortions due to susceptibility effects, we demonstrated that the correction technique with a true reversal of *k* space trajectory removes the majority of eddy current-induced distortion (see Fig. 7). If the applied diffusion-encoding gradient direction is held constant and *k* space traversal is reversed, then the frequency shift due to eddy currents caused by diffusion sensitization gradient switching will occur in the opposite direction with equal magnitude, and distortion will be opposing between pairs of images with opposite traversal. An important consideration here is whether both phase and frequency-encoding directions are reversed (Fig. 1a,b), or only phase-encoding direction is reversed (Fig. 1a,c). Failure to reverse-imaging gradients in both orientations will lead to incomplete eddy current distortion correction. In the complete *k* space trajectory reversal between Figure 1a,b, it can be seen that points 1 and 2 (and all other points) retain the same relative temporal positioning

during acquisition and therefore the same magnitude accumulation of phase error, leading to an exact reversal of spatial distortion. If only phase encoding is reversed, as between Figure 1a,c, then the temporal spacing of points in the k_y direction is also altered and an exact reversal of distortion does not occur. The above arguments are valid for eddy currents with time constants greater than the echo train acquisition window. In reality, some time-varying eddy current-induced field gradients are to be expected during the acquisition window, leading to varying image point spread function. Whilst this blurring effect is not corrected using the methods presented here, the gross image distortions caused by the nontime-varying component of the eddy current-induced gradients are simply and effectively removed. Our approach to correction of eddy current-induced distortions is distinct from the previous work of Bodammer and colleagues [Bodammer et al., 2004] who demonstrated similar gains by reversing the polarity of the diffusion-weighting gradients, rather than the k space trajectory. Although this previous work was effective at removing eddy current induced distortions it was ineffective for removing susceptibility-induced distortions.

An alternative method for obtaining a corrected image from opposite traversal k space image pairs has been described by Andersson et al. [2003]. These authors used basis functions to derive a corrected image form the original distorted pair by iteratively converging the images to each other. Although their method did appear to provide images with less distortion, we believe our implementation of the Bowtell method appears to give superior results with less apparent 'blurring' of the corrected image.

It has been suggested that distortion in diffusion-weighted sequences could be corrected by performing correction algorithms on $b = 0$ images and then using the derived pixel shift values to correct subsequent diffusion-weighted images [Huang et al., 2005; Lee et al., 2004]. Although subsequent images with the same or very similar intensity values could be corrected by this method, as for method C in the fMRI distortion correction described here, diffusion-weighted images may show very different intensity characteristics when compared with the $b = 0$ image, with inversion of relative contrast occurring in some areas (e.g., between CSF and tissue). With such differing signal intensity, the intense distortion occurring around sinuses, where signal from many neighboring voxels piles up into a single voxel, could not accurately be corrected by application of a pixel shift map derived from a $b = 0$ image pair as the information as to where the compressed diffusion-weighted signal should be remapped is simply not present, and a new mapping must be performed for each diffusion-weighted pair. In reality, if the same distortion map is applied to all the DW images then the resultant images may appear correct individually, with the boundary of the brain appearing in the same position in different direction weightings. If a fractional anisotropy map is produced from these images, it will however show a breakdown of structure within distorted areas as each diffusion-weighted image has the signal within the brain repositioned differently [Cercignani et al., 2007]. This is also the reason why attempts to correct susceptibility distortion in diffusion imaging by producing magnetic field maps and modeling the distortion will not work in areas of extreme signal pile up as there is no way to know what proportion of the compressed signal belongs to which true spatial position [Cercignani et al., 2007].

A major disadvantage of the dual k space traversal method is the requirement for two sets of images. This of course doubles imaging time and may limit the application of the technique where multiple sequences are required in an imaging protocol. The collection of two images does result in improved signal to noise (as discussed by Morgan et al. [2004] and it could be argued that it is preferable to obtaining data with two signal averages with the same distortion. It is hard to see how hardware developments in the immediate future could lead to significant reductions in the scan time, except maybe for greatly enhanced parallel imaging, although this itself will greatly reduce susceptibility related distortion by reducing the effective echo train length, thereby removing the need for the distortion correction algorithm.

Subsequent to the data described in this study, we have incorporated cardiac gating using a peripheral pulse unit positioned over the subject's index finger in accordance with previous recommendations [Jones and Pierpaoli, 2005]. This had the consequence of a further increase in imaging time, dependant on the subject's heart rate, but in the region of 16 min for each polarity acquisition.

If one wishes to apply diffusion-weighted tractography through regions subject to substantial magnetic susceptibility variation, then the distortion must be corrected. Ignoring the distortion will result in erroneous fiber-tracking results. With the acquisition parameters presented here at 3 T, geometric shifts in excess of 15 mm frequently occur in the temporal lobes, even when using a SENSE factor of 2.5. If these voxels represent part of a white matter tract then that part of the tract will have been wrongly positioned by this distance. In analogy with the arguments used to explain the need for diffusion vector reorientation during registration of DWI [Alexander et al., 2001], it is clear that displacement of part of a tract in this way will lead to invalidation of the directional coherence of diffusion orientation information. At successive points along the tract, the estimate of fiber orientations will no longer line up along the gross apparent orientation of the tract. This point is illustrated in Figure 8 using both a simulated tract and real diffusion vector plots obtained using the q ball method from one subject. After distortion correction has been applied, the vectors line up along a tract into the temporal lobe. The distortion correction greatly improves tracking through such areas as is clearly demonstrated in Figure 4 where the tract propagation is substantially enhanced in the distortion-corrected data. In the uncorrected tractography of Figure 4, the tract propagation

breaks down in the region of misplaced diffusion vectors indicated in Figure 8b.

Distortion-corrected fMRI acquisitions were achieved using three different methods. Of these, method C gave substantially greater activations in the FE analysis of data from 10 individuals performing a word categorization task. The higher levels of activation were evident as an increase in the number of significant activating regions, an increase in size of regions and also as higher *Z* statistic values within a significant activation coincident to all three methods. This method involved a brief prescan with interleaved dual direction *k* space traversal with the volunteer at rest, followed by the main time series over which the stimulus was applied. This method offers advantages in that the original TR is preserved in the corrected dataset (when compared with method A) and that the corrected dataset is not temporally shifted (in comparison with B). The recommendation would therefore be to proceed with method C, although comparisons on further subject data would be desirable. As dataset C used separate functional acquisitions to A and B, it is possible that the higher Z statistics and cluster number found were due to the underlying data, and not the distortion correction method, although five subjects underwent the imaging for method A and B first and five the imaging for C before A and B.

Comparison of group analysis of uncorrected and distortion corrected images from the same underlying dataset demonstrated that the distortion correction process did not adversely affect the statistics of the functionally analyzed data. One region of interest from an area of very high distortion in the inferior temporal lobe presented substantially higher *Z* statistics and volume in the corrected data. This suggested that in addition to correcting for misplacement of activation, the distortion correction could actually improve detection of activation in regions subject to substantial susceptibility related distortion. It has previously been reported that distortion correction of GE EPI functional time series improved statistical power of group studies [Cusack et al., 2003] due to an increase in the overlap of activation of different subjects. It has also been shown that distortion corrected datasets lead to improvements in registration [Hutton et al., 2002]. The substantial increase in activation found in Cluster 6 following distortion correction may not be due to improved registration alone. In addition to the inherent benefits in reducing signal loss of using SE-EPI (see below), this region of the inferior temporal lobe suffered severe distortion and compression in the original subject data, it is possible that uncompressing the signal in the region allowed signal increase associated with activation to cover a larger spatial area and therefore lead to increased statistical significance using cluster analysis.

Another possibility for producing distortion corrected activation maps would be to run the functional analysis on the uncorrected data and then attempt to transform the statistical maps into corrected space by application of an appropriate transform as in method C. Although it may be feasible to correct translation of statistical values by this method, it would be unfeasible to correctly remap the statistical values from regions subject to substantial susceptibility effect where compression or elongation of signal occur, as the remapped values would no longer have any true statistical meaning. Whatever the effects the distortion correction methods described here have on the final image sets, the statistical maps are valid for those distortion corrected datasets. As it has been shown that correction method C does not adversely affect *Z* statistic values when compared with the uncorrected data, and can indeed improve the statistics in highly distorted regions, the recommended procedure for further studies would be to acquire the data as described in acquisition 2 and correct it using method C. The prescan adds only a couple of minutes to overall scanning time.

The main functional time series in method C was corrected using maps of pixel shift derived from the prescan. It should be made clear that this method is not substantially different to any of the field map and/or registration-type corrections described in the literature [Chen and Wyrwicz, 1999; Jezzard and Balaban, 1995; Priest et al., 2006; Reber et al., 1998; Windischberger et al., 2004]. It is however simple to execute and we in effect map the distortion directly, rather than attempting to map the underlying magnetic field inhomogeneity and then calculate the resultant distortion.

A major driving factor behind this work was to use activations from functional imaging as direct seed regions for tractography. The results of tractography are extremely sensitive to seedpoint location, it was therefore essential to ensure that fMRI data, as well as diffusion data, were corrected for distortions and overlaid very accurately.

Although magnetic field map-based techniques can reposition misplaced signal, they cannot recover signal lost in GE EPI due to intravoxel dephasing. Methods to reduce and/or recover signal loss have been described including refocusing the gradient amplitude in the slice-select direction [Cordes et al., 2000] *z*-shimming [Deichmann et al., 2002; Du et al., 2007; Gu et al., 2002], and parallel imaging [Schmidt et al., 2005; Yang et al., 2004]. Although these approaches may reduce signal loss, they do not allow its full recovery in brain regions subject to the most substantial magnetic susceptibility effects. With respect to parallel imaging we use an eight-channel head coil and a SENSE acceleration factor of 2.5 in our functional acquisition, principally to reduce distortion and signal compression in the original images before application of the distortion correction algorithms. It must be emphasized that the use of a SE EPI sequence rather than a GE EPI sequence is a core factor in the success of applying our distortion corrected fMRI to areas of substantial magnetic susceptibility variation such as the temporal lobes. The SE refocusing pulse is arranged, so that the center of the echo train coincides with the center of the SE. At the center of the SE, phase shifts due to macroscopic field inhomogeneities are cancelled out resulting in less signal loss, although the image

distortions associated with narrow bandwidth in the phase encode direction remain. The signal characteristics of SE EPI are therefore dominated by T_2 rather than the T_2* of GE EPI, causing SE sequences to exhibit a smaller BOLD effect. In particular, the extra-vascular component of the BOLD signal around larger draining veins is much reduced with SE EPI [Bandettini et al., 1994]. Although this last effect causes a reduction in the overall BOLD effect and hence sensitivity to activation, it does have the beneficial consequence that measurement of hemodynamic activations with SE EPI should be better localized to regions of true metabolic activity.

Norris et al. [2002] compared GE EPI and SE EPI at 3 T using a color-word matching task known to produce robust activation in a number of regions. SE EPI was found to detect all activating regions detected with GE EPI and also detected two frontotemporal and ventral frontomedial activations not detected with GE EPI due to strong susceptibility gradients. They concluded that sensitivity at 3 T was sufficient to make SE EPI the method of choice for studies requiring a high degree of spatial localization.

Previous work using the word categorization task of this study revealed a small region of left temporal pole activation found when using PET but not with GE EPI fMRI. This lack of activation in the fMRI was considered to be an important indicator of susceptibility related signal loss [Devlin et al., 2000]. Examination of SE EPI functional data at a voxel level of $P < 0.01$ (uncorrected for multiple comparisons) indicates a region of activation in the left temporal pole in very close correspondence with that described from the PET data (circled in magenta, Fig. 12). Otherwise the SE EPI functional results of this study bear a close resemblance to those of Devlin et al. [2000] and demonstrate that SE EPI fMRI is sensitive enough to detect the higher order activity involved with such a task, even with a minimal data acquisition of 8 min per subject.

CONCLUSIONS

We have developed a robust algorithm for correcting magnetic susceptibility gradient and eddy current-induced distortion in DWI based upon the reversal of k space traversal and developments of the method of Bowtell et al. [1994]. This algorithm is accompanied by a modified acquisition to allow routine application to whole-brain high-angular resolution diffusion imaging. We demonstrate that distortions are detrimental to tractography results and that if single-shot PGSE EPI is to be used for diffusion-weighted tractography in regions subject to substantial susceptibility artefact then this distortion must be corrected to achieve meaningful results.

We applied variants of the distortion correction procedure to SE EPI fMRI acquisitions and achieved distortion corrected fMRI, free from the signal loss associated with intravoxel dephasing due to magnetic susceptibility variations. The distortion corrected functional data produced results comparable with previous functional studies using PET and GE EPI.

ACKNOWLEDGMENTS

We acknowledge the help of Liz Moore of Philips Medical Systems for assistance with sequence development.

REFERENCES

Alexander DC, Pierpaoli C, Basser PJ, Gee JC (2001): Spatial transformations of diffusion tensor magnetic resonance images. IEEE Trans Med Imaging 20:1131–1139.

Andersson JL, Skare S (2002): A model-based method for retrospective correction of geometric distortions in diffusion-weighted EPI. Neuroimage 16:177–199.

Andersson JL, Skare S, Ashburner J (2003): How to correct susceptibility distortions in spin-echo echo-planar images: Application to diffusion tensor imaging. Neuroimage 20:870–888.

Bammer R, Keeling SL, Augustin M, Pruessmann KP, Wolf R, Stollberger R, Hartung HP, Fazekas F (2001): Improved diffusion-weighted single-shot echo-planar imaging (EPI) in stroke using sensitivity encoding (SENSE). Magn Reson Med 46:548–554.

Bammer R, Auer M, Keeling SL, Augustin M, Stables LA, Prokesch RW, Stollberger R, Moseley ME, Fazekas F (2002): Diffusion tensor imaging using single-shot SENSE-EPI. Magn Reson Med 48:128–136.

Bandettini PA, Wong EC, Jesmanowicz A, Hinks RS, Hyde JS (1994): Spin-echo and gradient-echo EPI of human brain activation using BOLD contrast: A comparative study at 1.5 T. NMR Biomed 7:12–20.

Bodammer N, Kaufmann J, Kanowski M, Tempelmann C (2004): Eddy current correction in diffusion-weighted imaging using pairs of images acquired with opposite diffusion gradient polarity. Magn Reson Med 51:188–193.

Bowtell R, McIntyre DJO, Commandre M-J, Glover PM, Mansfield P (1994): Correction of Geometric Distortion in Echo Planar Images. Proc. 2nd Annual Meeting of the SMR, San Francisco, USA.

Cercignani M, Embleton KV, Parker GJ (2007): Comparison of distortion correction methods for EPI diffusion tensor MRI. Proc. 15th Annual Meeting of the ISMRM, Berlin, Germany.

Chang H, Fitzpatrick JM (1992): A technique for accurate magnetic resonance imaging in the presence of field inhomogeneities. IEEE Trans Med Imaging 11:319–329.

Chen NK, Wyrwicz AM (1999): Correction for EPI distortions using multi-echo gradient-echo imaging. Magn Reson Med 41:1206–1213.

Clare S, Evans J, Jezzard P (2006): Requirements for room temperature shimming of the human brain. Magn Reson Med 55:210–214.

Cordes D, Turski PA, Sorenson JA (2000): Compensation of susceptibility-induced signal loss in echo-planar imaging for functional applications. Magn Reson Imaging 18:1055–1068.

Cusack R, Brett M, Osswald K (2003): An evaluation of the use of magnetic field maps to undistort echo-planar images. Neuroimage 18:127–142.

Cusack R, Russell B, Cox SM, De Panfilis C, Schwarzbauer C, Ansorge R (2005): An evaluation of the use of passive

shimming to improve frontal sensitivity in fMRI. Neuroimage 24:82–91.

Deichmann R, Josephs O, Hutton C, Corfield DR, Turner R (2002): Compensation of susceptibility-induced BOLD sensitivity losses in echo-planar fMRI imaging. Neuroimage 15:120–135.

Devlin JT, Russell RP, Davis MH, Price CJ, Wilson J, Moss HE, Matthews PM, Tyler LK (2000): Susceptibility-induced loss of signal: Comparing PET and fMRI on a semantic task. Neuroimage 11(6, Pt 1):589–600.

Du YP, Dalwani M, Wylie K, Claus E, Tregellas JR (2007): Reducing susceptibility artifacts in fMRI using volume-selective z-shim compensation. Magn Reson Med 57:396–404.

Gu H, Feng H, Zhan W, Xu S, Silbersweig DA, Stern E, Yang Y (2002): Single-shot interleaved z-shim EPI with optimized compensation for signal losses due to susceptibility-induced field inhomogeneity at 3 T. Neuroimage 17:1358–1364.

Haroon HA, Morris DM, Embleton KV, Alexander DC, Parker GJ (2009): Using the model-based residual bootstrap to quantify uncertainty in fiber orientations from Q-ball analysis. IEEE Trans Med Imaging 28:535–550.

Haselgrove JC, Moore JR (1996): Correction for distortion of echo-planar images used to calculate the apparent diffusion coefficient. Magn Reson Med 36:960–964.

Huang H, Hua K, Jiang H, van Zijl PC, Mori S (2005): Characterization and correction of B0-susceptibility distortion in SENSE single-shot EPI-based DWI using manual landmark placement. Proc. 13th Annual Meeting of the ISMRM, Miami, USA.

Hutton C, Bork A, Josephs O, Deichmann R, Ashburner J, Turner R (2002): Image distortion correction in fMRI: A quantitative evaluation. Neuroimage 16:217–240.

Jezzard P, Balaban RS (1995): Correction for geometric distortion in echo planar images from B0 field variations. Magn Reson Med 34:65–73.

Jezzard P, Barnett AS, Pierpaoli C (1998): Characterization of and correction for eddy current artifacts in echo planar diffusion imaging. Magn Reson Med 39:801–812.

Jones DK, Pierpaoli C (2005). Contribution of cardiac pulsation to variability of tractography results. In: Proceedings of the International Society for Magnetic Resonance in Medicine, Miami Beech, Vol. 13.

Kybic J, Thevenaz P, Nirkko A, Unser M (2000): Unwarping of unidirectionally distorted EPI images. IEEE Trans Med Imaging 19:80–93.

Lee J, Lazar M, Holden J, Terasawa-Grilley E, Alexander AL (2004): Correction of Bo EPI distortions in diffusion tensor imaging and white matter tractography. In: Proceedings of the International Society for Magnetic Resonance in Medicine, Kyoto, Vol. 12. p 2172.

Liu G, Ogawa S (2006): EPI image reconstruction with correction of distortion and signal losses. J Magn Reson Imaging 24:683–689.

Miller KL, Pauly JM (2003): Nonlinear phase correction for navigated diffusion imaging. Magn Reson Med 50:343–353.

Morgan PS, Bowtell RW, McIntyre DJ, Worthington BS (2004): Correction of spatial distortion in EPI due to inhomogeneous static magnetic fields using the reversed gradient method. J Magn Reson Imaging 19:499–507.

Norris DG, Zysset S, Mildner T, Wiggins CJ (2002): An investigation of the value of spin-echo-based fMRI using a Stroop color-word matching task and EPI at 3 T. Neuroimage 15:719–726.

Ordidge RJ, Helpern JA, Qing ZX, Knight RA, Nagesh V (1994): Correction of motional artifacts in diffusion-weighted MR images using navigator echoes. Magn Reson Imaging 12:455–460.

Parker GJ, Alexander DC (2005): Probabilistic anatomical connectivity derived from the microscopic persistent angular structure of cerebral tissue. Philos Trans R Soc Lond B Biol Sci 360:893–902.

Parker GJ, Haroon HA, Wheeler-Kingshott CA (2003): A framework for a streamline-based probabilistic index of connectivity (PICo) using a structural interpretation of MRI diffusion measurements. J Magn Reson Imaging 18:242–254.

Preibisch C, Pilatus U, Bunke J, Hoogenraad F, Zanella F, Lanfermann H (2003): Functional MRI using sensitivity-encoded echo planar imaging (SENSE-EPI). Neuroimage 19(2, Pt 1):412–421.

Priest AN, De Vita E, Thomas DL, Ordidge RJ (2006): EPI distortion correction from a simultaneously acquired distortion map using TRAIL. J Magn Reson Imaging 23:597–603.

Reber PJ, Wong EC, Buxton RB, Frank LR (1998): Correction of off resonance-related distortion in echo-planar imaging using EPI-based field maps. Magn Reson Med 39:328–330.

Reinsberg SA, Doran SJ, Charles-Edwards EM, Leach MO (2005): A complete distortion correction for MR images. II. Rectification of static-field inhomogeneities by similarity-based profile mapping. Phys Med Biol 50:2651–2661.

Schmidt CF, Degonda N, Luechinger R, Henke K, Boesiger P (2005): Sensitivity-encoded (SENSE) echo planar fMRI at 3T in the medial temporal lobe. Neuroimage 25:625–641.

Studholme C, Constable RT, Duncan JS (2000): Accurate alignment of functional EPI data to anatomical MRI using a physics-based distortion model. IEEE Trans Med Imaging 19: 1115–1127.

Tuch DS (2004): Q-ball imaging. Magn Reson Med 52:1358–1372.

Tuch DS, Reese TG, Wiegell MR, Wedeen VJ (2003): Diffusion MRI of complex neural architecture. Neuron 40:885–895.

Visser M, Jefferies E, Lambon Ralph MA (2009): Semantic processing in the anterior temporal lobes: A meta-analysis of the functional neuroimaging literature. JoCN (in press). Available at: http://www.mitpressjournals.org/doi/pdf/10.1162/jocn.2009.21309.

Windischberger C, Robinson S, Rauscher A, Barth M, Moser E (2004): Robust field map generation using a triple-echo acquisition. J Magn Reson Imaging 20:730–734.

Yang QX, Wang J, Smith MB, Meadowcroft M, Sun X, Eslinger PJ, Golay X (2004): Reduction of magnetic field inhomogeneity artifacts in echo planar imaging with SENSE and GESEPI at high field. Magn Reson Med 52:1418–1423.

Yoder DA, Fitzpatrick JM, Paschal CB, Gatenby JC (2004): Exact correction of distortions due to static field inhomogeneities in spin echo echo planar imaging. In: Proceedings of the International Society for Magnetic Resonance in Medicine, Kyoto, Vol. 12.